Carbohydrate Polymers 92 (2013) 733–740

Contents lists available at SciVerse ScienceDirect

Carbohydrate Polymers

journal homepage: www.elsevier.com/locate/carbpol

Specific enzymatic tailoring of wheat arabinoxylan reveals the role of substitution on xylan film properties

Susanna L. Heikkinen[a,*], Kirsi S. Mikkonen[a], Kari Pirkkalainen[b], Ritva Serimaa[b], Catherine Joly[c], Maija Tenkanen[a]

[a] Department of Food and Environmental Sciences, P.O. Box 27, FIN-00014, University of Helsinki, Finland
[b] Department of Physics, P.O. Box 64, FIN-00014 University of Helsinki, Finland
[c] LRGIA EA 3733, Université de Lyon, Université Lyon 1, IUT DGB, 01000 Bourg en Bresse, France

ARTICLE INFO

Article history:
Received 16 April 2012
Received in revised form
21 September 2012
Accepted 28 September 2012
Available online 8 October 2012

Keywords:
Wheat arabinoxylan
Arabinofuranosidases
Branching
Film
Material properties

ABSTRACT

To increase understanding of the applicability of agro biomass by-products as biodegradable film formers, the effect of wheat arabinoxylan (WAX) fine structure on film properties was studied by applying specific enzyme modifications. WAX was selectively modified to mimic the natural variations of different arabinoxylans, particularly the degree of mono and disubstitution of α-L-arabinofuranosyl (Ara*f*) units in β-D-xylopyranosyl (Xyl*p*) backbone residues. The resulting modified WAX samples had similar arabinose-to-xylose (Ara/Xyl) ratios, but they differed in the number of unsubstituted Xyl*p* units. The substitution of WAX was found to affect, in particular, tensile strength, crystallinity, and oxygen permeability properties of the films, as statistically significant decreases in tensile strength and oxygen permeability took place after WAX de-branching. An increase in the number of unsubstituted Xyl*p* units decreased the temperature of relaxation of small-scale molecular motions of WAX (β-relaxation) and increased the degree of crystallinity of the films.

1. Introduction

Wheat (*Triticum* spp.) is the third most produced cereal in the world, after corn and rice, with a yearly production of over 600 million tonnes. By-products of cereal processing contain a large amount of xylans. For example, wheat bran and straw may contain up to 30% arabinoxylans (AXs) (Ebringerová, 2006; Sun, Lawther, & Banks, 1996). Cereal AXs consist of (1→4)-linked β-D-xylopyranosyl (Xyl*p*) backbone, to which α-L-arabinofuranosyl (Ara*f*) substituents are connected by (1→2)- and/or (1→3)-glycosidic linkages. Xylans may also carry acetyl and feruloyl groups, as well as α-D-glucopyranosyl uronic acid or its 4-*O*-methyl ether (Ebringerová & Heinze, 2000). Type and degree of substitution (DS) vary between species and between parts of the plant. In wheat, AX from endosperm and bran are more substituted than AX from straw. In wheat endosperm AX, the Ara/Xyl ratio may vary between 0.45 and 0.97 (Izydorczyk & Biliaderis, 1993). In wheat bran, composed primarily of aleurone and pericarp layers of grain, the Ara/Xyl ratio can be somewhat higher than in AX from wheat endosperm, varying from 0.57 to 1.07 (Shiiba, Yamada, Hara, Okada, & Nagao, 1993), whereas in less substituted wheat straw AX, the Ara/Xyl ratio is about 0.17 (Sun et al., 1996). In highly branched wheat arabinoxylan (WAX), such as from endosperm and bran, approximately two-thirds of the Ara*f* groups are attached in disubstituted Xyl*p* and one-third in monosubstituted Xyl*p* units (Fig. 1) (Pitkänen, Virkki, Tenkanen, & Tuomainen, 2009). Distribution of the Ara*f* substituents is not necessarily random over the xylan backbone, instead, alteration of highly and less branched parts in the AX chain is possible (Gruppen, Kormelink, & Voragen, 1993). AXs usually consist of populations, varying in molecular weight and type and degree of Ara*f* substitution, which can be fractionated by precipitation (Izydorczyk & Biliaderis, 1993).

Cereals contain both water-extractable and alkali-extractable (water-unextractable) arabinoxylans. The structures of alkaline- and water-extractable endosperm-derived WAXs are, however, rather similar (Gruppen et al., 1993). Water solubility of both alkaline and water-extracted AXs is affected by the Ara*f* substitution. Several studies indicate that water solubility generally increases when the number of Ara*f* substituents increases (Andrewartha, Phillips, & Stone, 1979; Pitkänen et al., 2009; Sternemalm, Höije, & Gatenholm, 2008; Zhang et al., 2011). Dervilly-Pinel, Thibault, and Saulnier (2001) suggested that arabinoxylans assume a semi-flexible conformation in water, and that differences in Ara/Xyl ratios do not affect the conformation or behavior of AX in solution. However, they concluded that the presence of Ara*f* residues,

* Corresponding author. Tel.: +358 9 191 58417; fax: +358 9 191 58475.
E-mail address: susanna.l.heikkinen@helsinki.fi (S.L. Heikkinen).

0144-8617/$ – see front matter © 2012 Elsevier Ltd. All rights reserved.
http://dx.doi.org/10.1016/j.carbpol.2012.09.085

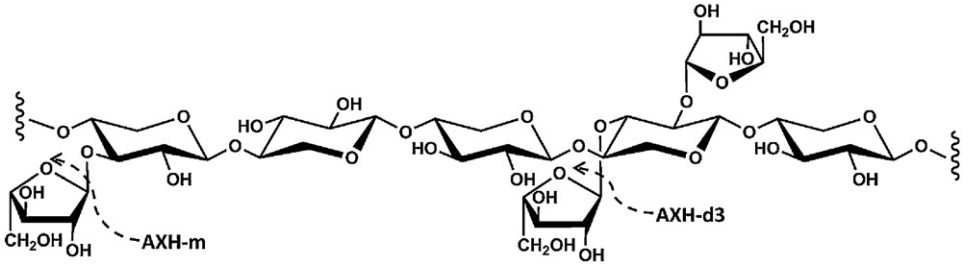

Fig. 1. Schematic chemical structure of wheat arabinoxylan and the removal of the α-L-arabinofuranosyl substituents by two distinct α-L-arabinofuranosidases AXH-m and AXH-d3.

as well as their distribution in the xylan backbone, might affect the interaction of AXs with each other, as well as with other cell wall components. Solution and hydrodynamic properties of WAX recently were shown to be affected by both the number of Ara*f* substituents present and the distribution of Ara*f* along the xylan chain (Pitkänen, Tuomainen, Virkki, & Tenkanen, 2011). In that study, no change in WAX conformation was detected when removing α-L-(1→3)-linked Ara*f* units from the disubstituted Xyl*p* residues. However, when WAX was de-branched from monosubstituted Xyl*p* residues, the water solubility decreased and, in DMSO, the de-branched chain seemed to have denser conformation than unmodified WAX. The effect of Ara*f* substitution on adsorption characteristics of WAX on cellulosic surface was also recently studied (Köhnke, Östlund, & Brelid, 2011). Specific enzymes are valuable tools in systematic structure–function studies. In both studies mentioned above, WAX was enzymatically tailored by specific α-L-arabinofuranosidases (EC 3.2.1.55), which hydrolyze terminal Ara*f* units from polymeric arabinoxylans. These arabinoxylan arabinofuranohydrolases (AXH) are divided into two groups, depending on their substrate specificities. The enzyme AXH-m acts on α-L-(1→2)- and (1→3)-linked Ara*f* units on monosubstituted Xyl*p* residues, whereas AXH-d3 releases only α-L-(1→3)-linked Ara*f* units from the disubstituted Xyl*p* residues (Fig. 1) (Van Laere, Beldman, & Voragen, 1997).

Utilization of agro biomass by-products, such as hemicelluloses in packaging materials, is an environmentally friendly alternative to oil-based products. Studies on the use of hemicelluloses (mainly xylans and mannans) as sustainable packaging material was recently reviewed by Hansen and Plackett (2008) and Mikkonen and Tenkanen (in press). An increasing number of studies on film formation of agro-based xylans, such as from cotton stalks, barley husks, oat spelt, corn hulls, and wheat bran, also indicate the importance of this research area (Bahcegul, Toraman, Ozkan, & Bakir, 2012; Höije, Gröndahl, Tommeraas, & Gatenholm, 2005; Mikkonen et al., 2009; Zhang & Whistler, 2004; Zhang et al., 2011). When the fine structure of rye AX (RAX) was modified, the content of Ara*f* substitution was found to affect the material and barrier properties of the films (Höije, Sternemalm, Heikkinen, Tenkanen, & Gatenholm, 2008; Mikkonen et al., 2012; Stevanic et al., 2011). The water solubility of RAX decreased and crystallinity of the films increased when Ara*f* substitution decreased. Zhang et al. (2011) observed that DS of wheat bran AX fractions affects thermal properties of the films. Our present study aimed to expand further the knowledge regarding the structure–function relationships of AX, especially that of wheat AX. We focused on the effect of both mono- and disubstitution of Xyl*p* units on WAX film properties. The degree and type of substitution of commercial, water-soluble WAX was systematically tailored by specific AXH treatments to mimic the structural variations of different native AXs. Film properties were studied extensively, covering both tensile and barrier properties, as well as morphology and sorption studies.

2. Materials and methods

2.1. Materials

Medium-viscosity wheat (*Triticum aestivum*) flour arabinoxylan (WAX, lots 40301b and 40302a) was purchased from Megazyme International (Wicklow, Ireland). The molecular weight (M_w) of medium-viscosity WAX was previously determined to be 213,900 g/mol (Pitkänen et al., 2009). The enzymes used were purified α-L-arabinofuranosidase (AXH-m, from *Meripilus giganteus*, GH51), kindly supplied by Novozymes (Bagsvaerd, Denmark), and α-L-arabinofuranosidase (E-AFAM2, AXH-d3, from *Bifidobacterium adolescentis*, GH43), purchased from Megazyme International. $Mg(NO_3)_2$, P_2O_5, and anhydrous $CaCl_2$ (granular size 1–2 mm) were obtained from Merck (Whitehouse Station, NJ).

2.2. Preparation of the films

The WAX was dissolved in deionized water (20 g/l) by magnetic stirring at 90–95 °C for 15 min. An equal volume of WAX solution and 50 mM sodium acetate buffer, pH 5.0, containing AXH-m (5000 nkat/g of AX) or 50 mM sodium phosphate buffer, pH 6.0, containing AXH-d3 (250 nkat/g of AX) were mixed and incubated at 40 °C for 48 h. A reference sample without enzyme addition (WAX-ref) was incubated in 25 mM sodium acetate buffer, pH 5.0, at 40 °C for 48 h. Enzyme action was terminated by keeping the solutions in boiling water for 15 min, after which the released arabinose was analyzed with a commercial kit (K-LACGAR; Megazyme, Wicklow, Ireland). The monosaccharide composition of WAX-ref was previously determined using gas chromatography after complete enzymatic hydrolysis (Virkki, Maina, Johansson, & Tenkanen, 2008). Ara/Xyl ratios of WAX-d3 and WAX-m were calculated by subtracting the content of released arabinose from the initial arabinose content and assuming that xylose content remains unaltered in the modifications. The specificity of the enzymes was shown in an earlier study (Pitkänen et al., 2011). Samples were dialyzed for 48 h (MWCO 12–14,000 Da), degassed by ultrasonication in vacuo for 5 min, and cast onto Teflon dishes (diameter 10 cm). WAX-ref, WAX-m, and WAX-d3 films were dried in a climate room at 23 °C and 50% RH. They were kept in those conditions at least seven days before measurement, except that the samples for dielectric analysis were conditioned under saturated $Mg(NO_3)_2$ at 54% RH, and the samples for water vapor sorption measurement were stored in vacuum desiccators over P_2O_5 at 0% RH. The thickness of the films was approximately 40–50 μm.

2.3. X-ray diffraction

Wide-angle X-ray scattering measurements of films were carried out in perpendicular transmission geometry, using Cu $K\alpha_1$ radiation (wavelength of 1.54 Å). A setup with a Rigaku rotating anode (fine focus) X-ray tube (Rigaku Corp., Tokyo, Japan)

and a MAR345 image plate detector (Rayonix, Evanston, IL) was used (Mikkonen et al., 2010). The beam was monochromated and focused on the detector with a bent Si (1 1 1) crystal and a totally reflecting mirror.

The recorded two-dimensional diffraction patterns were radially averaged to one-dimensional diffraction intensity profiles. The diffraction intensities were corrected to take into account the attenuation of radiation inside the sample and the differences in diffracted ray paths due to the flat detector. The angular range was calibrated using the known diffraction maxima of silver behenate, silicon, and aluminum standard samples. The broadening of the diffraction maxima due to the instrument was determined to be $0.37 \pm 0.1^\circ$ at 2θ of 31.6°, which was calculated from the 2 0 0 reflection of NaCl.

The diffraction intensities were plotted as a function of the scattering angle. The scattering angles are given in 2θ, which is twice the value of the Bragg angle in Bragg's law $\lambda = 2d_{hkl}\sin(\theta\,[^\circ])$. In the formula, λ is the wavelength of the incident radiation, and d_{hkl} is the distance of the planes given by Miller indices $h\,k\,l$.

The average xylan crystallite size B, in the direction normal to ($h\,k\,l$), was determined from the width of the $h\,k\,l$ reflection by using the Scherrer equation (Guinier, 1994; Patterson, 1939)

$$B_{hkl} = \frac{0.9\lambda}{\sqrt{(\Delta\theta)^2_{hkl} - (\Delta\theta)^2_{inst}}\cos(\theta_{hkl})} \quad (1)$$

where θ_{hkl} is the Bragg angle of the $h\,k\,l$ reflection, $(\Delta\theta)_{hkl}{}^2$ is the full width at half maximum (FWHM) of the $h\,k\,l$ reflection in radians and $(\Delta\theta)_{\mathrm{inst}}{}^2$ is the instrumental broadening in radians. In Eq. (1) the shape of the reflections is assumed to be Gaussian.

The X-ray diffraction measurements were carried out in ambient conditions of room temperature ($25 \pm 1\,^\circ$C) and relative humidity ($21 \pm 2\%$). Each diffraction pattern was accumulated for one hour. In order to acquire better intensity statistics, four films were stacked parallel to each other during diffraction measurements. Average sample thickness was 0.17 ± 0.02 mm.

2.4. Water sorption

A DVS Intrinsic sorption microbalance (Surface Measurement Systems, Alperton, UK) was used when studying the water sorption isotherms of the films. The measurements were carried out in triplicate at a humidity range of 0–90% and at 25 °C. The humidity was raised by steps of RH 10%. The sample weight was equilibrated at each step. The moisture uptake (%) was calculated according to Eq. (2):

$$\text{Moisture uptake} = 100\left[\frac{W_{\mathrm{moist}} - W_{\mathrm{dry}}}{W_{\mathrm{dry}}}\right] \quad (2)$$

where W_{moist} is the weight of the sample equilibrated at the chosen relative humidity, and W_{dry} is the weight of the dry sample.

2.5. Dielectric analysis

For dielectric testing, a TA Instruments Dynamic Electrical Analyzer (DEA 2970, TA Instruments, New Castle, DE) was used, in multi-frequency mode, as described previously (Zhang et al., 2011). Pre-hydrated films (RH 54%) were positioned between two electrodes. A Viton® gas barrier rubber O-ring seal was added between the sensor plates to prevent water evaporation during the measurement. Samples were measured as duplicates from −120 °C to +150 °C at a heating rate of 3 °C/min. Constant force (340 N) was applied during the experiment. The frequencies used were 1; 10; 100; 1000; 10,000; and 100,000 Hz. The peak temperatures of tangent delta at 1 Hz were taken as α- and β-relaxations (T_α and T_β), of which T_α was taken as glass transition temperature (T_g).

2.6. Tensile testing

Tensile testing was performed at 23 °C and 50% RH, using an Instron 4465 universal testing machine (Instron Corp., High Wycombe, England) with a load cell of 100 N to determine the tensile strength, elongation at break, and Young's modulus of the films. The initial grip distance was 50 mm, and the rate of grip separation was 5 mm/min. The specimen width was 10 mm, and the length was approximately 100 mm. The thickness of the films was measured with a micrometer (Lorentzen & Wettre, Kista, Sweden; precision 1 μm) at five points, and the average was calculated. Twelve replicate specimens of each film type were measured.

2.7. Water vapor permeability

The water vapor permeability (WVP) of the films was determined in triplicate with an RH gradient of 0/54%. Films were sealed on aluminum cups containing 43 g $CaCl_2$ to give 0% RH. There was an air gap of 6 mm between $CaCl_2$ and the underside of the film. The cups were placed in a desiccator cabinet equipped with a fan; the relative humidity was maintained at 54% with saturated $Mg(NO_3)_2$ solution. The temperature in the cabinet was 22 °C, and the air velocity above the samples was 0.15 m/s. The cups were weighed once a day, for a total of five times. The temperature and RH of the cabinet were measured before each weighing with a Rotronic HygroPalm RH meter (Bassersdorf, Switzerland). The water vapor transmission rate (WVTR) was calculated from the linear regression of the slope of weight gain versus time by dividing the slope by the test cell mouth area. The water vapor partial pressure at the underside of the film was calculated with the correction method described by Gennadios, Weller, and Gooding (1994). The WVP was obtained by multiplying the WVTR by the thickness of the film, and then dividing that by the water vapor partial pressure difference between the two sides of the film. The thickness of the film was measured at ten points at 1-μm precision prior to testing.

2.8. Oxygen permeability

The oxygen gas transmission rate (OTR) of the films was measured using an Ox-Tran Twin equipped with coulometric sensor (Modern Controls, Inc., Minneapolis, MN). Four replicates of the films were measured at 22 °C and RH 50–75%. The film area was 5 cm^2, and the thickness of the film was measured at five points at 1-μm precision. Oxygen permeability (OP) was calculated by multiplying OTR by film thickness, and then dividing that by the oxygen gas partial pressure difference between the two sides of the film.

2.9. Statistical analysis

One-way analysis of variance (ANOVA) was used to test the differences in tensile properties of the films. Tukey's test was used for pairwise comparison of the means. A *t*-test was used to compare the differences in WVP and OP results. Differences were considered statistically significant when p was ≤ 0.05. SPSS 15.0.1 (SPSS Inc., Chicago, IL) was used for the analysis.

3. Results and discussion

3.1. Enzymatic tailoring

The effect of branching on WAX film properties was studied by applying two selective α-L-arabinofuranosidases, AXH-m and AXH-d3, with different substrate specificities. The efficient action and specificity of these enzymes on WAX was previously verified by ^{1}H NMR spectroscopy (Pitkänen et al., 2011; Sørensen et al., 2006). The enzyme dosages were chosen after preliminary studies. The

Fig. 2. Schematic presentation of structures of (a) untreated WAX (WAX-ref, Ara/Xyl 0.56), (b) AXH-d3 treated WAX (WAX-d3, Ara/Xyl 0.34), and (c) AXH-m treated WAX (WAX-m, Ara/Xyl 0.29). X = xylopyranosyl residue, A = arabinofuranosyl residue.

maximum removal of Ara*f* units from monosubstituted Xyl*p* was obtained by using the AXH-m at a dosage of 5000 nkat/g, and the maximum removal of Ara*f* from disubstituted Xyl*p* was obtained by using the AXH-d3 at a dosage of 250 nkat/g, both incubated for 48 h at 40 °C. Both enzymes worked efficiently, as they were able to remove about one-third of the Ara*f* groups, resulting in Ara/Xyl ratios of 0.29 (WAX-m) and 0.34 (WAX-d3) (Fig. 2). These values were calculated by comparing the amount of liberated Ara to the Ara*f* content of WAX without enzyme treatment (WAX-ref, Ara/Xyl 0.56; Virkki et al., 2008). The amount of unsubstituted Xyl*p* of all Xyl*p* residues was calculated based on the Ara/Xyl ratios when the specificity of AXH-m and AXH-d3 is known (Pitkänen et al., 2011) and was 66% in the unmodified WAX-ref, and 66% and 86% in WAX-d3 and WAX-m, respectively (Table 1).

The removal of Ara*f* units from monosubstituted Xyl*p* residues decreased the water solubility of WAX, resulting in partial precipitation of WAX-m in film solution. The same effect was seen earlier when RAX and WAX were treated with AXH-m; it was considered to be due to the intermolecular aggregation of unsubstituted parts of the xylan chain (Höije et al., 2008; Köhnke et al., 2011; Pitkänen et al., 2011). This hypothesis is supported by the fact that the removal of one of the Ara*f* groups from doubly substituted Xyl*p* units did not affect the water solubility of the WAX-d3, although the Ara/Xyl ratio decreased significantly. All samples formed cohesive, self-supporting films without the addition of an external plasticizer; however, the films from WAX-m were more brittle and translucent than the other films.

3.2. Crystallinity

Crystallinity of the WAX films was determined, as a previous study with RAX indicated that crystallinity increased when RAX was de-branched with AXH-m (RAX-m), and increased crystallinity was associated with increased mechanical performance and decreased oxygen permeability of the films (Höije et al., 2008). No detailed studies on WAX film crystallinity have been published previously. In this study, the intensities and diffraction maxima were used to identify the crystal structure of xylan, calculate the lattice parameters, and evaluate the relative amount of crystalline and amorphous regions of xylan present in the samples. The 100% crystalline xylan diffraction pattern was calculated using the known crystal structure and atomic coordinates of xylan dihydrate (Nieduszynski & Marchessault, 1972), and the 0% crystalline pattern (i.e., amorphous or non-crystalline background) was measured from the WAX-ref film. The calculated diffraction pattern was then compared with the measured intensity profiles, and the lattice parameters, *a* and *c* of the hexagonal crystal structure, were refined to fit the measured diffraction maxima.

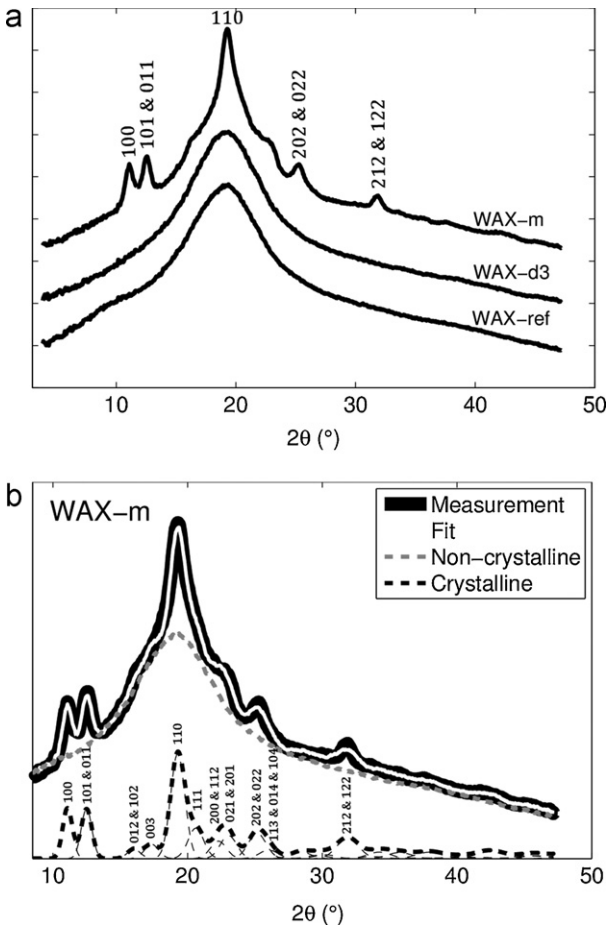

Fig. 3. (a) Average radial X-ray diffraction patterns of WAX samples. The curves for WAX-d3 and WAX-m have been shifted vertically for easier visualization. (b) Average radial X-ray diffraction pattern of WAX-m sample and crystallinity fit. The Miller indices *h k l* of the most relevant reflections are shown above the respective diffraction maxima.

Table 1
Ara/Xyl ratios, the amount of unsubstituted xylose units of the WAX films, T_β, and T_g. T_β and T_g were measured at 1 Hz, RH 54%.

	Ara/Xyl	Unsubstituted Xyl*p* units (%)[a]	T_β (°C)	T_g (°C)
WAX-ref	0.56	66	−100.3 ± 2.9	40.4 ± 0.5
WAX-d3	0.34	66	−100.9 ± 2.0	52.2 ± 2.6
WAX-m	0.29	86	−105.6 ± 0.4	40.6 ± 0.3

[a] Calculated from Ara/Xyl ratios when the specificity of AXH-m and AXH-d3 is known.

Crystallinity analysis indicated that the xylan in the sample WAX-m (Ara/Xyl 0.29) was semi-crystalline (crystallinity of 12 ± 3%); i.e., there were regions of xylan crystallites surrounded by amorphous regions. Diffraction maxima, corresponding to the xylan dihydrate reflections 1 0 0, 1 0 1 and 0 1 1, 1 1 0, 2 0 2 and 0 2 2 and 2 1 2 and 1 2 2, were observed in the intensity pattern (Fig. 3). By using the widths of the diffraction maxima (the 1 1 0 reflection of xylan dihydrate) and the Scherrer equation (Eq. (1)), the average size of single xylan crystallites in this study was determined to be 8.2 ± 0.6 nm, which is similar to crystallite size 6.3 ± 0.3 nm of xylan in RAX-m film determined previously (Stevanic et al., 2011). The azimuthal distribution of the observed reflections in the two-dimensional intensity pattern was isotropic, which indicates that the xylan crystallites in sample WAX-m had no preferred

orientation in the plane of the film. The diffraction pattern of the sample WAX-d3 (Ara/Xyl 0.34) was quite similar to that of the amorphous reference sample (Ara/Xyl 0.56) and showed no distinct diffraction maxima. Thus, the xylan in the sample is assumed to have no long-range crystalline order. The results are shown in Fig. 3.

AX films with low Ara/Xyl ratio, such as those from barley husk AX, with an Ara/Xyl ratio of 0.22, were previously shown to be semi-crystalline (Höije et al., 2005). Crystallinity of RAX-m films increased with decreasing Ara/Xyl ratio; however, the degree of crystallinity was not determined (Höije et al., 2008). The degree of crystallinity of the RAX-m films was determined to be 11 ± 2% when the Ara/Xyl ratio was 0.27 (Mikkonen et al., 2012) and 20 ± 3% after more intensive de-branching, resulting in an Ara/Xyl ratio of 0.16 (Stevanic et al., 2011). In addition, glycerol- and sorbitol-plasticized oat spelt AX films with an Ara/Xyl ratio of 0.14 were semi-crystalline, with a degree of crystallinity of 20–26% (Mikkonen et al., 2009). In WAX-m (Ara/Xyl 0.29), 86% of Xyl*p* units are unsubstituted (Table 1), and in RAX-m (Ara/Xyl 0.27), 80% of Xyl*p* units are unsubstituted (Pitkänen et al., 2011), resulting in a similar degree of crystallinity, 12 ± 3% and 11 ± 2%, respectively. RAX and WAX have similar Ara/Xyl ratios (about 0.50), but distribution of Ara*f* branches between mono- and disubstituted Xyl*p* residues is reversed, RAX having roughly two-thirds of the Ara*f* units in monosubstituted Xyl*p* residues and one-third in disubstituted Xyl*p*; so RAX has less unsubstituted Xyl*p* residues than WAX (Pitkänen et al., 2011). The present results are in agreement with the previous studies where the increase in the amount of the unsubstituted parts of the xylan chain enhanced the formation of xylan crystallites in the film structure. It is noteworthy that when Ara*f* groups were removed from the disubstituted Xyl*p* units, the film structure remained amorphous. Thus, not only does the Ara/Xyl ratio affect the crystallinity of AXs, but also the distribution of Ara*f* units along the xylan backbone.

3.3. Thermal properties

Thermal relaxations in the amorphous phase of the films were examined using DEA. As stated above, WAX-ref and WAX-d3 films were amorphous, whereas WAX-m film contained crystalline areas (12%), whose molecular motion is very low and are not shown in this analysis. Two relaxations (α and β) were observed in all films. At sub-ambient temperatures, small-scale molecular motions are released and are defined as β-relaxation (T_β) (Butler & Cameron, 2000). At higher temperatures, the mobility of large xylan chain segments increases and is defined as α-relaxation (glass transition, T_g). In our study, T_β values of WAX-ref and WAX-d3 films were similar, but T_β of WAX-m film was significantly lower than that of the other two (Table 1). The correlation between the degree of Ara*f* substitution and T_β of the WAX film was recently reported by Zhang et al. (2011). They concluded that when Xyl*p* units are highly substituted with Ara*f*, local mobility of WAX in the films decreases and T_β increases. Results in our study indicate that the number of substituted Xyl*p* units, rather than DS of WAX, affects the local molecular mobility of WAX in the amorphous part of the films. The T_β values of the films from the two de-branched WAXs studied differed, although their Ara/Xyl ratios were similar; however, the amounts of substituted Xyl*p* units were different. In addition, the Ara/Xyl ratios of WAX-ref and WAX-d3 were different, but their T_β values were similar. AXH-d3 releases only one of the Ara*f* units in doubly substituted Xyl*p*, so the number of unsubstituted Xyl*p* units does not increase after AXH-d3 treatment.

The α-relaxation (T_g) of WAX-d3 film, on the other hand, clearly took place at a higher temperature than that of WAX-m and WAX-ref films (Table 1). At T_g, the molecular mobility increases and material becomes more flexible. At RH 50%, all the studied films contained approximately 12% water (Fig. 4), which acts as a plasticizer affecting the T_g (Ying, Barron, Saulnier, & Rondeau-Mouro, 2011). Higher T_g value obtained for WAX-d3 (52.2 °C) than for WAX-ref (40.4 °C) indicates that mobility of xylan chains decreases when the number of disubstituted Xyl*p* units decreases. Removal of Ara*f* substituents from monosubstituted Xyl*p* units led to partial crystallization of unsubstituted areas of WAX-m, but amorphous areas presumably still contained disubstituted Xyl*p* units. Below T_g, amorphous material is in a glassy state, meaning that it is more brittle and the movement of the molecules is more restricted. According to DEA measurements, all samples studied herein were in a glassy state at room temperature at RH ≤ 54%. In this study similar T_g values were obtained for WAX-ref and WAX-m. This result is in accordance with a previous study by Stevanic et al. (2011), in which the T_g of RAX did not change significantly after removal of all Ara*f* groups from monosubstituted Xyl*p* units. Ying et al. (2011) studied T_g of WAX film with DSC, where midpoint of the heat capacity change was 82 °C at RH 59%. Their result is higher than the temperature of α-relaxation observed in the present study. WAX used in their study contained ferulic acid, had an Ara/Xyl ratio of 0.73, and the percentage of unsubstituted Xyl*p* units was 56%.

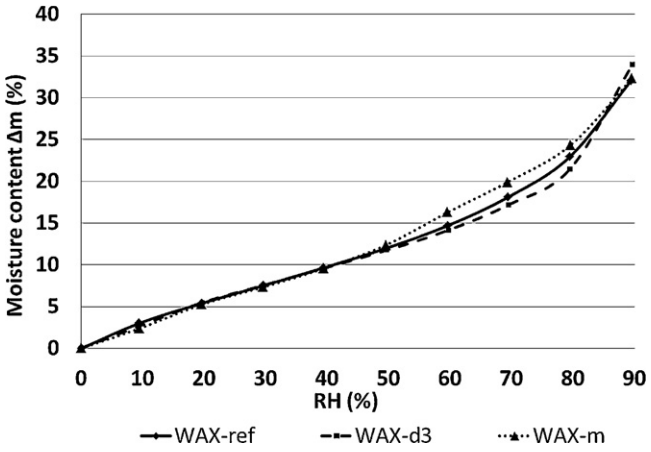

Fig. 4. Water sorption isotherms of the WAX films (moisture content Δ*m* (%) versus RH 0–90%). Results are averages of three measurements.

3.4. Water sorption

The shape of the water sorption isotherm of all films was sigmoidal (Fig. 4). At RH 0–50%, the isotherms were almost identical, but above RH 50%, there were small differences. There was no variation between parallel measurements of each film, so the differences between film types are not due to experimental variation. Semi-crystalline WAX-m films absorbed more water than the amorphous WAX-ref and WAX-d3 films at RH 50–80%; however, at RH 90%, the moisture uptake of WAX-d3 films was somewhat higher than that of the other films. In previous studies, films from the most substituted AX absorbed most water at RH 98%; however, under RH 80%, the amount of absorbed water decreased when the Ara/Xyl ratio increased (Höije et al., 2008; Sternemalm et al., 2008). Zhang et al. (2011) found that below RH 80%, the differences between the wheat bran AX films with varying Ara/Xyl ratios were small, whereas above RH 80%, water uptake of films increased notably, due to swelling by water; the results correlated well with DS. In this study, however, we did not detect a significant increase in water uptake above RH 80%, which is in accordance with the water vapor sorption results of Ying et al. (2011). As stated in Section 3.3, all samples studied here were in a glassy state at room temperature at RH 0–54%. In a glassy state, water sorption is typically surface adsorption, but when the relative humidity increases, the plasticizing effect of water increases, inducing glass

transition, where the molecular mobility increases, allowing water to absorb to the amorphous material (Burnett, Malde, & Williams, 2009). In this study, sorption isotherms of samples differed above RH 50%, which might be due to differences between molecular mobility of chemically different WAX in films, detected using DEA.

3.5. Mechanical properties

Mechanical properties were determined at RH 50% and 23 °C, where all studied films were in a glassy state. This can be seen as high tensile strength and low elongation at break of the films. In all films in the present study, the amount of plasticizing water was the same, as the water content of the films was similar at RH 50% (Fig. 4). WAX-ref film had a tensile strength of 40 MPa, which is somewhat lower than that reported for the structurally different RAX 53 MPa (Höije et al., 2008), corn hull AX 54 MPa (Zhang & Whistler, 2004), and barley husk AX 50 MPa (Höije et al., 2005), but higher than oat spelt AX film with 10% of glycerol as plasticizer 28 MPa (Mikkonen et al., 2009). Elongation at break of WAX-ref film was 6.5%, which is similar to more branched corn hull AX (6.2%), but higher than those of RAX (4.7%), barley husk (2.5%). Stiffness of the WAX-ref film was the lowest, with Young's modulus of 990 ± 120 MPa, compared to those of RAX (1750 ± 740 MPa), corn hull AX (1316 ± 90 MPa), and barley husk (2930 ± 300 MPa). These cereal AXs differ both in their molecular weight (M_w) and Ara/Xyl ratios; however, neither of these properties alone clearly explains the differences in tensile strength. For instance, M_w of barley husk is 36,000 g/mol and Ara/Xyl 0.22 (Höije et al., 2005), whereas M_w of corn hull AX is 506,000 g/mol and Ara/Xyl 0.56 (Zhang & Whistler, 2004); however, their reported tensile strengths are similar. The effect of molecular weight on tensile properties was previously studied by Mikkonen et al. (2012), who found that tensile strengths and Young's modulus of the films from RAXs with an Ara/Xyl ratio of about 0.45 were similar, regardless of M_w (184,000 g/mol and 49,000 g/mol).

De-branching of WAX affected the tensile properties of the films. The WAX-ref film with the highest Ara/Xyl ratio was the strongest, while both de-branched WAX films (WAX-m and WAX-d3) had a lower tensile strength (Fig. 5a). Interestingly, there were no differences in the tensile strength results, whether the de-branching was from monosubstituted Xyl*p* unit or disubstituted Xyl*p* unit, although the former had a semi-crystalline structure and the latter was amorphous. Our results indicate that high number of Ara*f* units in Xyl*p* residues has beneficial influence on tensile strength of films. Similar effect was seen earlier when RAX-films were studied (Höije et al., 2008). Interactions between the xylan chains with lower DS seemed to decrease the tensile strength. In the semicrystalline WAX-m film, the decrease in the tensile strength could be due to inadequate interactions between the crystalline and amorphous parts. However, the water solubility of WAX and the crystallinity of the film did not explain the decreased tensile strength of amorphous WAX-d3 films. The decreased tensile strength in WAX-d3 films might be partially due to the differences in the molecular mobility of the xylan chains as indicated by differences in the α-relaxation temperature (T_g) of the WAX-ref and in WAX-d3 films (Table 1), depending on the amount of Ara*f* substituents attached to the xylan backbone. During film formation and drying, when there is still water in the system and the forming film is in a rubbery state, the xylan chains with different DS might orientate differently, according to their ability to move. However, more studies are needed to better understand this phenomenon. The elongation at break of the film from WAX-d3 did not differ significantly from that of the WAX-ref film (Fig. 5b). Elongation at break was lowest in the WAX-m film (Fig. 5b); this film had clear precipitation and it was semi-crystalline, which probably reduced the ability of WAX chains to slide across each other. On the other hand, semi-crystalline WAX-m had similar Young's modulus to that of the WAX-ref film, approximately 1000 MPa (Fig. 5c). In contrast, treatment of WAX with AXH-d3 decreased the Young's modulus of films to 800 MPa, indicating that the removal of Ara*f* groups from disubstituted Xyl*p* units decreased the stiffness of the films. De-branching of WAX affected the tensile strength of films similarly to de-branching of RAX in a previous study (Höije et al., 2008); in both cases, tensile strength decreased when Ara/Xyl ratio decreased. However, de-branching of WAX by AXH-m decreased the elongation at break of WAX-m films, whereas elongation at break of RAX-m films was higher than that of the unmodified RAX film. DS and Ara/Xyl ratios of unmodified WAX and RAX are similar, but the substitution pattern is different which might affect the mechanical properties.

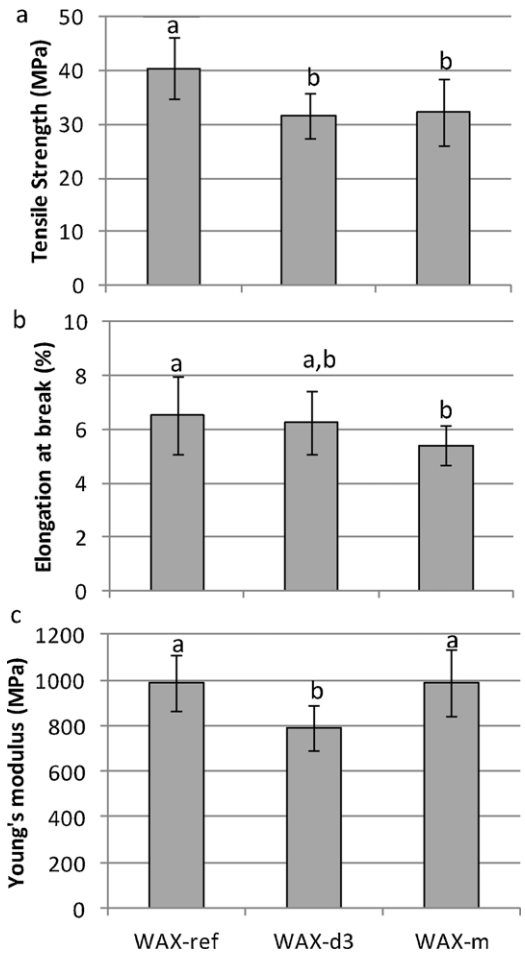

Fig. 5. (a) Tensile strength, (b) elongation at break, and (c) Young's modulus of WAX-ref, WAX-d3, and WAX-m, measured with Instron tensile tester. The results are averages of 10–12 measurements, and the error bars indicate standard deviations. Lower-case a and b signify statistically significant differences from Tukey's test ($p \leq 0.05$).

3.6. Water vapor and oxygen gas permeability

The WVP and OP were determined on WAX-ref and WAX-d3 films. Unfortunately, these analyses were not successful on WAX-m film, due to possible pinholes in the film, leading to leaking of oxygen and water vapor through the film. WAX-m films were semi-crystalline, and crystalline structures usually lower permeability (McHugh & Krochta, 1994). However, in this study, where no external plasticizer was used, the decreased water solubility of WAX-m led to partial aggregation of film solution, making the film brittle, which may have increased the pinhole formation or otherwise broken the film during removal from the dish.

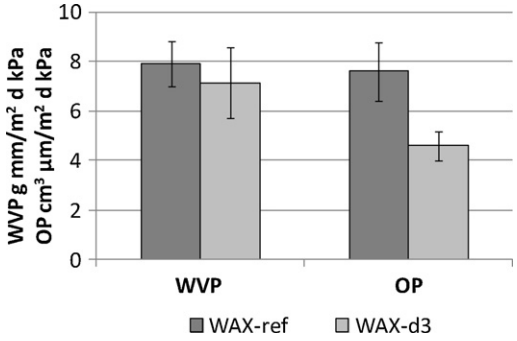

Fig. 6. Water vapor permeability (WVP, RH 0/54%) and oxygen permeability (OP, RH 50–75%) of WAX-ref and WAX-d3 films. WVP results are averages of three measurements; OP results are averages of four measurements. The error bars indicate standard deviation.

The OP decreased significantly ($p \leq 0.05$) when the Ara/Xyl ratio was decreased by AXH-d3, keeping the amount of substituted Xyl*p* units the same; however, the effect was not statistically significant in WVP (Fig. 6). Both of the studied films were amorphous, their moisture uptake was similar, and, according to DEA measurements, the mobility of xylan chains in both films was low at the conditions used in the permeability measurements. The OP results in this study indicate that removal of one Ara*f* from the disubstituted Xyl*p* leads to more dense packing of xylan chains, thereby decreasing the permeability of oxygen gas. In the WVP results, however, no significant differences were observed between the reference and de-branched samples. Cereal AX films, like other polysaccharide films, are sensitive to water; however, only some WVP results of AX films can be found in the literature. Water-extracted rye bran arabinoxylan film had a WVP of 7.7 [(g mm)/(kPa m^2 d)] (Sárossy, Tenkanen, Pitkänen, Bjerre, & Plackett, 2013), which was similar to the WVPs of this study, where the WVP of WAX-ref was 7.9 [(g mm)/(kPa m^2 d)] and the WVP of WAX-d3 was 7.2 [(g mm)/(kPa m^2 d)]. Lower values were obtained with plasticized films. For example, the WVP for the oat spelt AX with 10% glycerol was 3.3 [(g mm)/(kPa m^2 d)], and with 10% sorbitol it was 1.1 [(g mm)/(kPa m^2 d)] (Mikkonen et al., 2009). The WVP of corn hull AX also decreased when plasticizer was added; no plasticizer 4.1 [(g mm)/(kPa m^2 d)], and with 13% sorbitol 2.0 [(g mm)/(kPa m^2 d)] (Zhang & Whistler, 2004). The effect of AX structure on WVP has not previously been evaluated.

In the previous study with de-branched RAX, semicrystalline films were successfully measured, and an increase in de-branching, with a concomitant increase in crystallinity, was found to decrease the OP (Höije et al., 2008). Crystalline areas in the films were expected to increase the length of the diffusion path of oxygen gas and, therefore, lower the permeability. In this study, no crystalline areas were observed in the WAX-d3 films, and yet the OP decreased significantly compared to WAX-ref film. The OP of the RAX film at RH 50% was 2 [(cm^3 µm)/(m^2 d kPa)] (Höije et al., 2008), which is lower than that of WAX film, 7.6 [(cm^3 µm)/(m^2 d kPa)], determined in this study. However, both films had OPs lower than 10 [(cm^3 µm)/(m^2 d kPa)], which is regarded as the limit for a good oxygen barrier (Krochta & De Mulder-Johnston, 1997). RAX is naturally low in disubstituted Xyl*p* residues (Pitkänen et al., 2011), whereas, in this study, we decreased the number of disubstituted Xyl*p* residues by a specific enzyme (AXH-d3), resulting in a 40% decrease in OP. The OP values of cereal-based AX films have been reviewed recently by Mikkonen and Tenkanen (in press). The lowest OP reported for the cereal-derived AX films at RH 50% is that for barley husk AX, 0.16 [(cm^3 µm)/(m^2 d kPa)], having an Ara/Xyl ratio of 0.22 and most of the substituted Xyl*p* carrying a single Ara*f* residue (Höije, 2008; Höije et al., 2005).

4. Conclusions

By applying targeted enzymatic modification, we were able to show that the substitution pattern affects material properties of films prepared from wheat arabinoxylan. Although the length of Ara*f* branches in WAX is only one monosaccharide unit, their distribution over the backbone defines the morphology of the film. The number of unsubstituted Xyl*p* units was found to affect water solubility of WAX and lead to increased crystallinity of the WAX-m film. This study clearly shows that changes in Ara*f* substitution have different effects on mechanical, thermal, and barrier properties. Thus, the fine structure of AX has relevance when various agricultural side-streams are considered as raw materials for film applications. Optimally structured AX can be aimed by selective fractionation techniques of biomass or specific enzymatic modifications of isolated AX, as shown in the present study.

Acknowledgements

We would like to thank Miguel Pernes from INRA Reims France for DEA measurements, and Dr. Kirsti Parikka from the University of Helsinki for drawing the WAX structure (Fig. 1). We also thank the University of Helsinki Research Funds and the Academy of Finland (contract no. 132150) for their financial support.

References

Andrewartha, K. A., Phillips, D. R., & Stone, B. A. (1979). Solution properties of wheat-flour arabinoxylans and enzymatically modified arabinoxylans. *Carbohydrate Research*, *77*, 191–204.

Bahcegul, E., Toraman, H. E., Ozkan, N., & Bakir, U. (2012). Evaluation of alkaline pretreatment temperature on a multi-product basis for the co-production of glucose and hemicellulose based films from lignocellulosic biomass. *Bioresource Technology*, *103*, 440–445.

Burnett, D., Malde, N., & Williams, D. (2009). Characterizing amorphous materials with gravimetric vapour sorption techniques. *Pharmaceutical Technology Europe*, *21*, 41–45.

Butler, M. F., & Cameron, R. E. (2000). A study of the molecular relaxations in solid starch using dielectric spectroscopy. *Polymer*, *41*, 2249–2263.

Dervilly-Pinel, G., Thibault, J. F., & Saulnier, L. (2001). Experimental evidence for a semi-flexible conformation for arabinoxylans. *Carbohydrate Research*, *330*, 365–372.

Ebringerová, A. (2006). Structural diversity and application potential of hemicelluloses. *Macromolecular Symposia*, *232*, 1–12.

Ebringerová, A., & Heinze, T. (2000). Xylan and xylan derivatives—biopolymers with valuable properties. *Macromolecular Rapid Communications*, *21*, 542–556.

Gennadios, A., Weller, C. L., & Gooding, C. H. (1994). Measurement errors in water vapor permeability of highly permeable, hydrophilic edible films. *Journal of Food Engineering*, *21*, 395–409.

Guinier, A. (1994). *X-ray diffraction in crystals, imperfect crystals, and amorphous bodies*. New York: Dover Publications Inc.

Gruppen, H., Kormelink, F. J. M., & Voragen, A. G. J. (1993). Water-unextractable cell wall material from wheat flour: 3. A structural model for arabinoxylans. *Journal of Cereal Science*, *18*, 111–128.

Hansen, N. M. L., & Plackett, D. (2008). Sustainable films and coatings from hemicelluloses: A review. *Biomacromolecules*, *9*, 1493–1505.

Höije, A. (2008). *Bioprocessing, structure and material properties of arabinoxylans*. Doctoral thesis. Gothenburg, Sweden: Chalmers University of Technology.

Höije, A., Gröndahl, M., Tømmeraas, K., & Gatenholm, P. (2005). Isolation and characterization of physicochemical and material properties of arabinoxylan from barley husk. *Carbohydrate Polymers*, *61*, 266–275.

Höije, A., Sternemalm, E., Heikkinen, S., Tenkanen, M., & Gatenholm, P. (2008). Material properties of films from enzymatically tailored arabinoxylans. *Biomacromolecules*, *9*, 2042–2047.

Izydorczyk, M. S., & Biliaderis, C. G. (1993). Structural heterogeneity of wheat endosperm arabinoxylans. *Cereal Chemistry*, *70*, 641–646.

Krochta, J. M., & De Mulder-Johnston, C. (1997). Edible and biodegradable polymer films: Challenges and opportunities. *Food Technology*, *51*, 61–74.

Köhnke, T., Östlund, Å., & Brelid, H. (2011). Adsorption of arabinoxylan on cellulosic surfaces: Influence of degree of substitution and substitution pattern on adsorption characteristics. *Biomacromolecules*, *12*, 2633–2641.

McHugh, T. H., & Krochta, J. M. (1994). Permeability properties of edible films. In J. M. Krochta, E. A. Baldwin, & M. Nisperos-Carriedo (Eds.), *Edible coatings and films to improve food quality* (pp. 139–183). Lancaster, PA: Technomic Publishing Company.

Mikkonen, K. S., & Tenkanen, M. Sustainable food-packaging materials based on future biorefinery products: Xylans and mannans. *Trends in Food Science and Technology*, in press, http://dx.doi.org/10.1016/j.tifs.2012.06.012

Mikkonen, K. S., Heikkinen, S., Soovre, A., Peura, M., Serimaa, R., Talja, R. A., et al. (2009). Films from oat spelt arabinoxylan plasticized with glycerol and sorbitol. *Journal of Applied Polymer Science*, *114*, 457–466.

Mikkonen, K. S., Mathew, A. P., Pirkkalainen, K., Serimaa, R., Xu, C., Willför, S., et al. (2010). Glucomannan composite films with cellulose nanowhiskers. *Cellulose*, *17*, 69–81.

Mikkonen, K. S., Pitkänen, L., Liljeström, V., Bergström, E., Serimaa, R., Salmén, L., et al. (2012). Arabinoxylan structure affects the reinforcement of films by microfibrillated cellulose. *Cellulose*, *19*, 467–480.

Nieduszynski, I. A., & Marchessault, R. H. (1972). Structure of β,D(1→4′)-xylan hydrate. *Biopolymers*, *11*, 1335–1344.

Patterson, A. L. (1939). The diffraction of X-rays by small crystalline particles. *Physical Review*, *56*, 978–982.

Pitkänen, L., Virkki, L., Tenkanen, M., & Tuomainen, P. (2009). Comprehensive multidetector HPSEC study on solution properties of cereal arabinoxylans in aqueous and DMSO solutions. *Biomacromolecules*, *10*, 1962–1969.

Pitkänen, L., Tuomainen, P., Virkki, L., & Tenkanen, M. (2011). Molecular characterization and solution properties of enzymatically tailored arabinoxylans. *International Journal of Biological Macromolecules*, *49*, 963–969.

Sárossy, Z., Tenkanen, M., Pitkänen, L., Bjerre, A.-B., & Plackett, D. (2013). Extraction and chemical characterization of rye arabinoxylan and the effect of β-glucan on the mechanical and barrier properties of cast arabinoxylan films. *Food hydrocolloids*, *30*, 206–216. http://dx.doi.org/10.1016/j.foodhyd.2012.05.022

Shiiba, K., Yamada, H., Hara, H., Okada, K., & Nagao, S. (1993). Purification and characterization of two arabinoxylans from wheat bran. *Cereal Chemistry*, *70*, 209–214.

Sternemalm, E., Höije, A., & Gatenholm, P. (2008). Effect of arabinose substitution on the material properties of arabinoxylan films. *Carbohydrate Research*, *343*, 753–757.

Stevanic, J. S., Joly, C., Mikkonen, K. S., Pirkkalainen, K., Serimaa, R., Rémond, C., et al. (2011). Bacterial nanocellulose-reinforced arabinoxylan films. *Journal of Applied Polymer Science*, *122*, 1030–1039.

Sun, R., Lawther, J. M., & Banks, W. B. (1996). Fractional and structural characterization of wheat straw hemicelluloses. *Carbohydrate Polymers*, *29*, 325–331.

Sørensen, H. R., Jørgensen, C. T., Hansen, C. H., Jørgensen, C. I., Pedersen, S., & Mayer, A. S. (2006). A novel GH43 α-L-arabinofuranosidase from *Humicola insolens*: Mode of action and synergy with GH51 α-L-arabinofuranosidases on wheat arabinoxylan. *Applied Microbiology and Biotechnology*, *73*, 850–861.

Van Laere, K. M. J., Beldman, G., & Voragen, A. G. J. (1997). A new arabinofuranohydrolase from *Bifidobacterium adolescentis* able to remove arabinosyl residues from double-substituted xylose units in arabinoxylan. *Applied Microbiology and Biotechnology*, *47*, 231–235.

Virkki, L., Maina, H. N., Johansson, L., & Tenkanen, M. (2008). New enzyme-based method for analysis of water-soluble wheat arabinoxylans. *Carbohydrate Research*, *343*, 521–529.

Ying, R., Barron, C., Saulnier, L., & Rondeau-Mouro, C. (2011). Water mobility within arabinoxylan and β-glucan films studied by NMR and dynamic vapour sorption. *Journal of the Science of Food and Agriculture*, *91*, 2601–2605.

Zhang, P., & Whistler, R. L. (2004). Mechanical properties and water vapor permeability of thin film from corn hull arabinoxylan. *Journal of Applied Polymer Science*, *93*, 2896–2902.

Zhang, Y., Pitkänen, L., Douglade, J., Tenkanen, M., Remond, C., & Joly, C. (2011). Wheat bran arabinoxylans: Chemical structure and film properties of three isolated fractions. *Carbohydrate Polymers*, *86*, 852–859.